

The preparation of porous graphite and its application in lithium ion batteries as anode material

Tianshu Deng¹ · Xiaoping Zhou¹

Received: 4 March 2016 / Revised: 17 May 2016 / Accepted: 22 May 2016 / Published online: 28 May 2016
© Springer-Verlag Berlin Heidelberg 2016

Abstract Graphite is the most widely used anode material for lithium ion batteries (LIBs). However, the performance of graphite is limited by its slow charging rates. In this work, porous graphite was successfully prepared by nickel-catalyzed gasification. The existence of the pores and channels in graphite particles can greatly increase the number of sites for Li-ion intercalation-deintercalation in graphite lattice and reduce the Li-ion diffusion distance, which can greatly facilitate the rapid diffusion of lithium ions; meanwhile, the pores and channels can act as buffers for the volume change of the graphite in charging-discharging processes. As a result, the prepared graphite with pores and channels exhibits excellent cycling stability at high rate as anode materials for LIBs. The porous graphite offers better cycling performance than pristine graphite, retaining 81.4 % of its initial reversible capacity after 1500 cycles at 5 C rates. The effective synthesis strategy might open new avenues for the design of high-performance graphite materials. The porous graphite anode material is proposed in applications of high rate charging Li-ion batteries for electric vehicles.

Keywords Nickel catalyst · Porous graphite · Anode material · Lithium ion batteries

Introduction

Lithium ion batteries (LIBs) are currently the vital power sources for portable electronic devices and electric vehicles

✉ Xiaoping Zhou
hgx2002@hnu.edu.cn

¹ Department of Chemical Engineering, Hunan University, Chang, Hunan 410082, People's Republic of China

[1, 2]. In vehicle applications, the charging rate of the LIB is the crucial character, because it is not feasible for electric vehicle (EV) users to wait several hours to charge the vehicles.

Graphite has been the most commonly used anode material owing to its high energy density and low cost [3, 4]. However, the narrow interlayer spaces (0.335 nm) and the long diffusion distance of lithium ions in graphite crystals results in high lithium ion diffusion resistance. A high charging rate can lead to the fatal growth of lithium dendrites on the graphite surface [5, 6]. In order to improve the electrochemical performance of graphite, various strategies of modification methods were applied in graphite preparation, i.e., the surface oxidation [7, 8], the surface fluorination [9], the metal coating [10, 11], and the carbon coating [12]. These modifications could usually accelerate the electrochemical reaction rates of the graphite, reduce the surface active species, and reduce the initial irreversible capacity of batteries. However, these modifications could not improve the lithium diffusion rate in graphite particles. Because lithium ions intercalate-deintercalate from the edges of graphite layers, the larger the graphite crystals are, the slower the lithium ions intercalate-deintercalate into/from the graphite. In order to accelerate the lithium ion diffusion process, creating pores and channels in graphite crystals may be an effective approach to accelerate lithium ion diffusion rate; additionally, the pores and channels could buffer the volume change of graphite in the charging-discharging cycles.

Catalytic gasification of graphite in oxygen [13], hydrogen [14], carbon dioxide [15], and steam [16] by various metal and metal oxide catalysts has been well studied. However, these artificial porous graphite materials were rarely tested as anode materials in LIBs. Our primary investigation on this topic was published as a letter (in which molybdenum oxide was selected as the catalyst to create pores or channels in graphite) [17]. In this work, more detail investigations on the preparation

and characterization of porous graphite as anode material were conducted. The preparation reaction was shown in Scheme 1.

Experimental

Synthesis of porous graphite

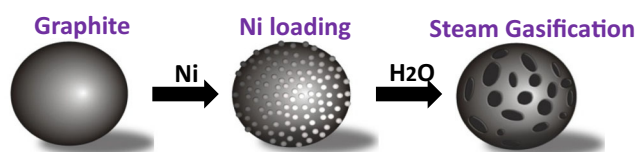
Commercial graphite (GHMG-M G0812, 1500 g, Chuang Ya Inc.) was added into a $\text{Ni}(\text{NO}_3)_2$ solution (3500 g, containing 8.85 g of $\text{Ni}(\text{NO}_3)_2 \cdot 6\text{H}_2\text{O}$) under stirring. After stirring for 1 h, the solution was dried in a spray dryer (180 °C) to obtain a powder sample. The powder sample was placed into a tube furnace and heated to 800 °C at a ramp rate of 5 °C/min in N_2 . After the temperature was stabilized at 800 °C, liquid water was pumped into the tube furnace with desired flows. In the preparation of porous graphite PG-0.1, the flow of water (liquid) was 0.10 ml/min, while in the preparation of porous graphite PG-0.2, the flow of water (liquid) was 0.20 ml/min. After 15 h of reaction, the water pump was turned off and the furnace was cooled down to room temperature under N_2 flow to obtain the porous graphite.

Characterization of porous graphite

The morphological and structural information was obtained from a scanning electron microscope (SEM, FE-SEM S-4800, Hitachi) equipped with an energy-dispersive X-ray spectrometer (EDS). The specific surface areas (SSA) of the samples were measured with an automated gas adsorption apparatus (Micromeritics, ASPS 2020), using liquid nitrogen as an adsorbent at 77 K. The size distribution of small pores in graphite was measured by argon (87.3 K) adsorption (Quantachrome Autosorb iQ MP). The laser Raman spectra of the graphite materials were collected by using a JY HR800 Raman spectrometer (Horiba Jobin Yvon, France) with a 532-nm diode laser excitation. The X-ray diffraction (XRD) characterization of the sample was conducted by using an X-ray diffraction meter (Rigaku D/Max-rA, CuK radiation).

Electrochemical measurements

Coin cell: the negative electrodes of cells were prepared by coating a copper foil with a slurry of anode material. The mass loading of the anode material on copper foil was 2.3 mg/cm².



Scheme 1 The preparation of porous graphite

The slurry of the anode material was prepared from pristine graphite or porous graphite, conductive carbon, and polyvinylidene fluoride (PVDF) binder (dispensed in N-methyl-2-pyrrolidone) with a weight ratio of 85:5:10. The coin-type half cells (2025) were prepared in a helium-filled glove box with Li metal as counter electrode. The other materials used in the preparation of the cells were the polyethylene separator and the LiPF_6 electrolyte solution (1.2 M in ethylene carbonate (EC)/ethyl methyl carbonate (EMC) with a weight ratio of 3/7).

Batteries (with a capacity of 3.0 Ah, electrode area 14.4 cm × 6.9 cm) were prepared by using $\text{LiNi}_{0.4}\text{Co}_{0.2}\text{Mn}_{0.4}\text{O}_2$ as the cathode material and the pristine graphite or porous graphite as the anode material. The cathode was prepared by coating the aluminum foil with the slurry comprising the $\text{LiNi}_{0.4}\text{Co}_{0.2}\text{Mn}_{0.4}\text{O}_2$ material, carbon black (as a conducting additive), and a PVDF binder (dispersed in N-methyl-2-pyrrolidone) with a weight ratio of 85:5:10. The $\text{LiNi}_{0.4}\text{Co}_{0.2}\text{Mn}_{0.4}\text{O}_2$ loading was 27.3 mg/cm². The anode was prepared by coating the copper foil with the slurry prepared from porous graphite (or pristine graphite), conductive carbon, and a PVDF binder (dispensed in N-methyl-2-pyrrolidone) with a weight ratio of 85:5:10. The mass loading of anode material was 10.8 mg/cm². The prepared cathode, anode, PE separator, and electrolyte solution (LiPF_6 (1.2 M) in EC/EMC (3/7)) were used to assemble the batteries.

In the charge-discharge test, the batteries were charged at 3.0 A (1 C), 9.0 A (3 C), and 15.0 A (5 C) and discharged at 9.0 A (3 C). The charge-discharge potential was between 2.5 and 4.2 V. In order to shorten the testing time, the charge-discharge tests of the batteries were conducted at 45 °C (high temperature could accelerate the degradation rate of the batteries to shorten the testing time).

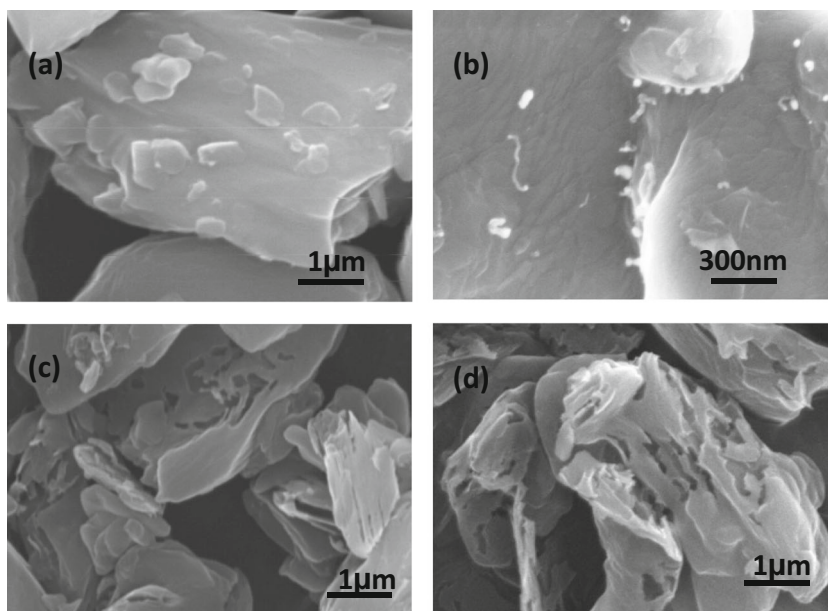
Electrochemical impedance spectroscopy (EIS) was collected on an AUTOLAB PGSTAT302N (Metrohm). The impedance spectra were recorded by applying an AC voltage of 5 mV in the frequency range from 1 MHz to 0.01 Hz.

Results and discussion

Characterizations of the materials

The morphologies of the graphite materials are shown in Fig. 1. The SEM pictures show that the pristine graphite has a smooth surface (Fig. 1a), the pristine graphite loaded with $\text{Ni}(\text{NO}_3)_2$ and heated in N_2 at 500 °C has NiO_x nanocrystals over the surface (Fig. 1b), and the graphite samples after gasification catalyzed by Ni catalysts in steam (liquid H_2O 0.10 ml/min in Fig. 1c and liquid H_2O 0.20 ml/min in Fig. 1d) at 800 °C have pores in the graphite particles. The results indicate that the Ni catalyst (which catalyzes the steam gasification of graphite at 800 °C) is much more

Fig. 1 SEM images untreated and treated graphite. **a** Pristine graphite; **b** graphite supported Ni(NO₃)₂ after annealed at 500 °C under N₂ flow (G-500); **c** porous graphite (PG-0.1) obtained after the steam gasification of graphite at 800 °C for 15 h, when the water flow was 0.10 ml/min. **d** Porous graphite (PG-0.2) obtained after the steam gasification of graphite at 800 °C for 15 h, when the water flow was 0.20 ml/min



active than the molybdenum oxide catalyst (which catalyzes the steam gasification of graphite at 900 °C) [17]. In all the cases, the pores and channels are in micrometer level, which could be effectively wetted by electrolyte solution.

The data in Table 1 show that following the reaction of graphite with water steam at 800 °C in the presence of Ni catalyst, the specific surface area (SSA) of graphite increased (from 1.93 m²/g to a maximum of 4.18 m²/g), while the tap density (TD) of graphite decreased. These results indicate that the pores and channels had been created in the graphite particles. With the increase of the H₂O flow from 0.10 to 0.20 ml/min, more graphite was gasified, corresponding to more weight loss of graphite. Also, with the increase of H₂O flow, the SSA of graphite increased, while the TD of graphite decreased. However, even higher H₂O flow (0.30 ml/min) did not lead to further apparent changes in SSA and TD. The argon adsorption measurements also show that, in contrast with the pristine graphite, pores with size greater than 25 nm (Fig. 2) were well developed in PG-0.1. These pores should be accessible by an electrolyte solution.

The X-ray diffraction patterns of the pristine graphite and the PG-0.1 are shown in Fig. 3a. It is found that the PG-0.1 has a strong diffraction peak at 26.5° (002) with the d₀₀₂ (the interlayer distance of graphite) equals to 3.36 Å, which is

Table 1 The effect of water flow on weight loss of graphite (WLG), SSA, and TD

sample	H ₂ O (ml/min)	WLG (%)	SSA (m ² /g)	TD (g/ml)
pristine graphite			1.93	0.98
PG-0.1	0.10	9.0	3.83	0.90
PG-0.2	0.20	13.1	4.13	0.82
PG-0.3	0.30	15.2	4.18	0.82

close to the d₀₀₂ value (3.35 Å) of the pristine graphite. This result indicates that the porous graphite PG-0.1 has the same lattice structure as that of the pristine graphite. Hence, the graphite lattice structure is still retained in PG-0.1.

Raman spectroscopy has been used to characterize carbon materials owing to its high sensitivity to the defects and disorders of the graphite lattice, with these structural features monitored through the characteristics of the G band and D band [18]. The D band is related to the breathing mode of the A_{1g} symmetry, corresponding to carbon atoms at the edges and defects. On the other hand, the G band is attributed to the E_{2g} symmetry that is associated with the ordered sp² bonded carbons. Figure 3b shows the Raman spectra of the pristine graphite and the porous graphite. A G band at 1580/cm and a D band at 1328/cm are observed on both of graphite materials. The ID/IG (intensity of D band/intensity of G band) ratio of the porous graphite is 0.33, while that of the pristine graphite

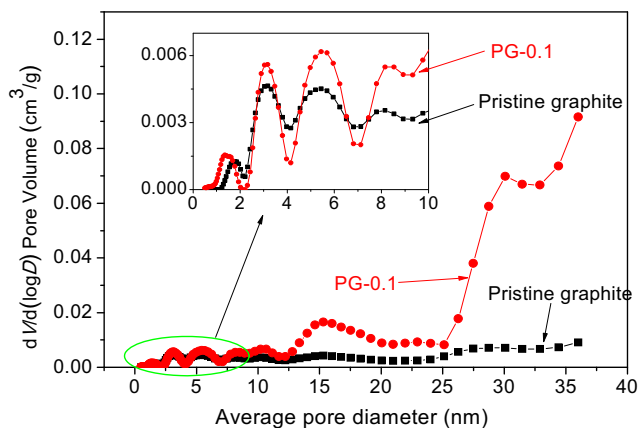
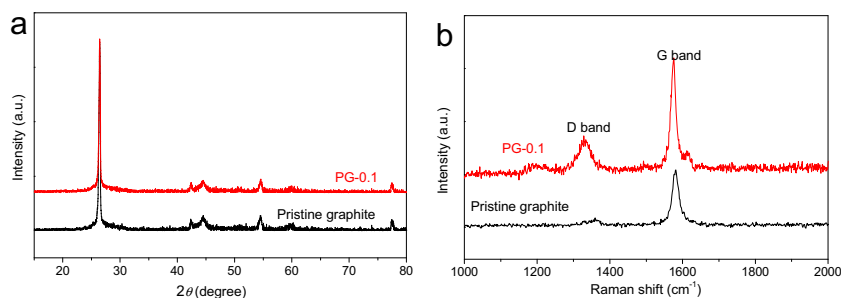


Fig. 2 The pore size distribution of pristine graphite and PG-0.1. The inset is the detailed view in the circle

Fig. 3 The XRD patterns and Raman spectra of pristine sample and PG-0.1. **a** XRD patterns; **b** Raman spectra



is 0.17. The results indicate that the edges and defects are well developed in porous graphite.

Electrochemical test

Table 2 gives the initial capacities and initial coulombic efficiencies of the coin cells prepared from pristine graphite, PG-0.1, and PG-0.2. Clearly, PG-0.1 and PG-0.2 have even higher initial discharge capacities than that of the pristine graphite. The reason could be that the porous graphite could accommodate more lithium ions in the nano-pores of the porous graphite [19]. However, the PG-0.1 and PG-0.2 have relatively lower initial coulombic efficiencies than that of the pristine graphite. This may be due to the presence of larger number of the edges and defects in the porous graphite (Raman characterization), leading to more irreversible lithiation of the anode. However, after the first charge-discharge cycle, almost 100 % of coulombic efficiencies were reached in the following charge-discharge cycles for all of the materials.

The results of Fig. 4 show that the discharge voltage of PG-0.2 is higher than that of PG-0.1 and the discharge voltage of PG-0.1 is higher than that of the pristine graphite. However, in the charging process, a reverse voltage order was observed at a current density of 100 mA/g. The results indicate that the lithium ion diffusion resistance in the porous graphite is smaller than that in the pristine graphite. This may be due to the pores in the porous graphite offering extra pathways for lithium ion intercalation into the graphite crystals.

Figure 5 gives the cycling performances of the batteries (designed as 3 Ah) prepared from the pristine graphite, the PG-0.1, and the PG-0.2. After the batteries were cycled 850 cycles at a charging rate of 1 C (3.0 A) and a discharging

Table 2 The initial capacities and efficiencies of pristine graphite, PG-0.1, and PG-0.2 at current density of 35 mA/g

Cell	Initial discharge (mAh/g)	Reversible (mAh/g)	Irreversible (mAh/g)	Initial efficiency
Pristine graphite	360.9	325.3	35.6	90.1 %
PG-0.1	403.3	350.0	53.3	86.8 %
PG-0.2	403.7	346.1	57.6	85.3 %

rate of 3 C (9.0 A), batteries prepared from the pristine graphite, the PG-0.1, and the PG-0.2 retained 79.9, 88.5, and 88.4 % of capacities, respectively (Fig. 5a). However, when the batteries were charged at 3 C and discharged at 3 C, the batteries prepared from PG-0.1 and PG-0.2 have much longer cycling life than that prepared from pristine graphite, and the battery prepared from PG-0.2 have even better performance than that prepared from PG-0.1 (Fig. 5b). When the batteries were charged at even higher rate (5 C), the battery prepared from PG-0.2 has the best performance. Even after 1500 charge-discharge cycles, the PG-0.2 battery still retained 81.4 % of its original capacity. However, at the same test conditions, the battery prepared from pristine graphite could only be cycled less than 200 cycles in retaining more than 80 % of its original capacity (Fig. 5c). These results indicate that the high charging rate leads to fatal damage to the pristine graphite. For the purpose of easy comparison, the performances of PG-0.2 batteries at charging rates of 1, 3, and 5 C are plotted together in Fig. 5d. The results show that these batteries have almost the same good cycling stability, although they were charged at different rates. The results indicate that the batteries prepared from the porous graphite are much more stable than that prepared from the pristine graphite, especially when the batteries were charged at a high rate.

Nyquist plots of the batteries prepared from pristine graphite and PG-0.2 after three charge-discharge cycles are shown in Fig. 6. The Nyquist plots are composed of a semicircle in a

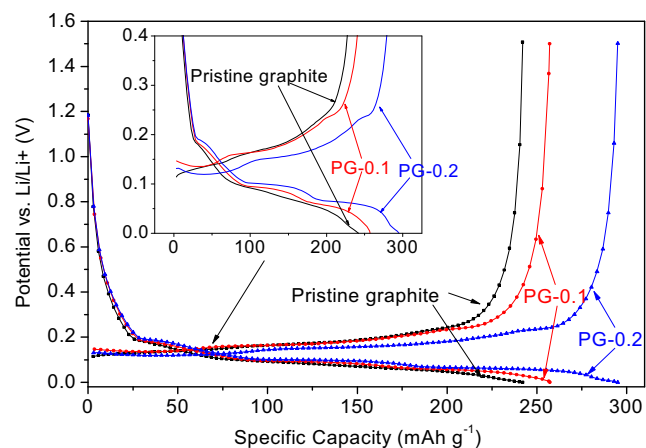
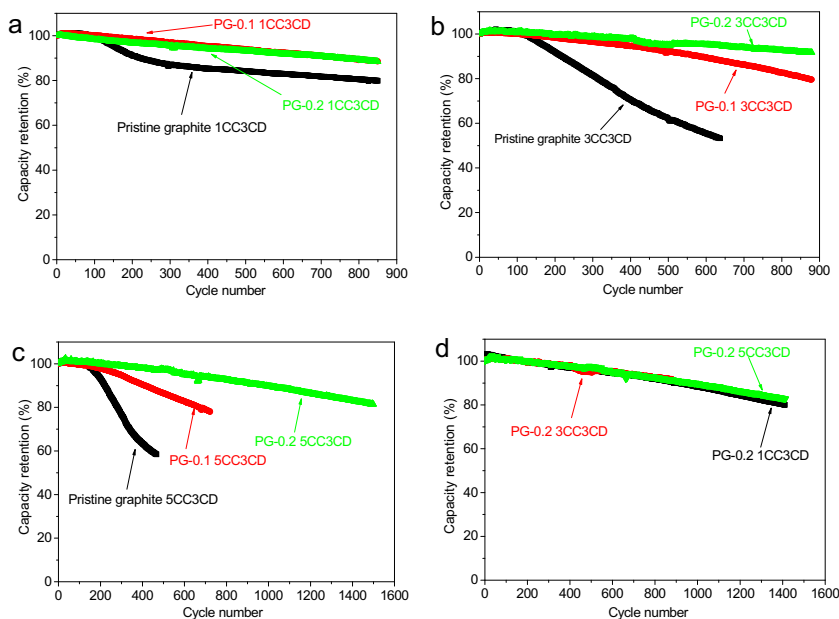


Fig. 4 Discharge-charge curves of pristine sample, PG-0.1, and PG-0.2 at a current density of 100 mA/g. The inset is the detailed view

Fig. 5 The cycling performances of batteries prepared from pristine graphite, PG-0.1, and PG-0.2 at different rates at 45 °C. **a** Charged at 1 C and discharged at 3 C; **b** charged at 3 C and discharged 3 C; **c** charged at 5 C and discharged at 3 C; **d** PG-0.2 batteries charged at 1, 3, and 5 C and discharged at 3 C



high-frequency region and a sloping line in the low-frequency region. An equivalent circuit (inset of Fig. 6) was used to analyze the measured impedance data [20, 21], where R_s represents the total resistance of electrolyte, electrode, and separator. R_{SEI} and CPE_1 are the resistance and capacitance of the SEI formed on the electrode, respectively. R_{ct} and CPE_2 represent the charge-transfer resistance and the double layer capacitance, respectively. Z_w is the Warburg impedance. The fitting values along with this equivalent circuit are presented in Table 3. As can be seen, the R_{SEI} and R_{ct} of the PG-0.2 battery are 1.26 and 8.45 m Ω , respectively, which are much smaller than that of the pristine graphite electrodes, indicating that both SEI resistance and charge transfer resistance of porous graphite are significantly reduced. The results indicate

that the well-developed porous system in the porous graphite offers extra approaches for Li-ion intercalation-deintercalation. Hence, the surface resistance is reduced.

It is known that the diffusion time of lithium ions in graphite lattice is proportional to the square of the diffusion length (L) ($t \propto L^2/D$) (D is the lithium ion diffusion coefficient) [22, 23]. The SEM pictures of Fig. 1 indicate that, in the pristine graphite, the diffusion length of lithium ions is estimated to be the radius (averagely 5 μm), while in the porous graphite, the diffusion length of lithium ions sometimes could be smaller than 2 μm . In the porous graphite, many pathways (the pores and channels in graphite) can be filled in by the electrolyte solution and the diffusion distance of lithium ions in the graphite lattice is greatly shortened, and the pores and

Fig. 6 Nyquist plots of the batteries (3.0 Ah) prepared from pristine graphite and PG-0.2 (the inset is the equivalent circuit used to fit the experimental curves)

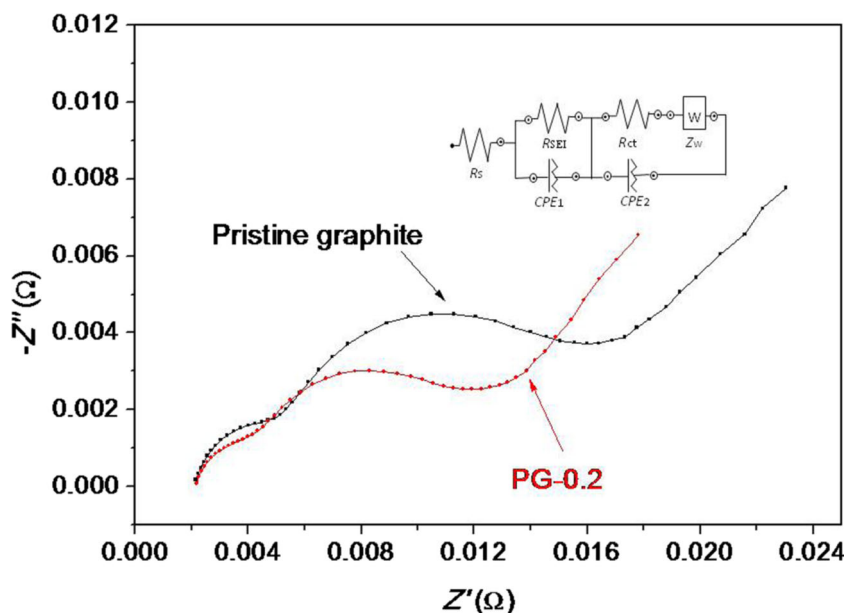


Table 3 The values of the equivalent circuit components obtained by fitting the experimental curves

Sample	R_s (m Ω)	R_{SEI} (m Ω)	R_{ct} (m Ω)
Pristine graphite	2.22	2.32	11.2
PG-0.2	2.27	1.26	8.45

channels in graphite particles can greatly increase the number of sites for Li-ion intercalation-deintercalation, which can greatly facilitate the rapid diffusion of lithium ions in graphite particles. In addition to the favorable diffusion kinetics of lithium ions in graphite particles, the pores and channels in graphite can also act as buffers for volume change when batteries are in charge-discharge cycles (because graphite exhibits a volume change of approximately 10 % during the battery charge-discharge cycles. The layered structure of graphite can be broken after many cycles of charging-discharging [24]). Hence, the pores and channels created in graphite also contribute to the stabilization of the graphite structure. The above reasons explained why the batteries prepared from porous graphite exhibits excellent cycling stability at high charge-discharge rates.

Conclusion

In summary, graphite with pores and channels was fabricated by the nickel-catalyzed steam gasification of graphite. The existence of the pores and channels in graphite particles can greatly shorten the intercalation-deintercalation distance of Li-ions in graphite lattice and reduce the SEI resistance and charge transfer resistance of graphite. Hence, the pores and channels in graphite particles facilitate the rapid diffusion of lithium ions in graphite, and also, the pores and channels act as buffers for the volume change in the charge-discharge processes of batteries. These reasons might explain why batteries with porous graphite anodes showed longer cycling life at high charging rate (5 C) than that with the pristine graphite anode. This means that low cost and simple method of producing the porous graphite can effectively improve the electrochemical properties of graphite. Batteries using the as-

prepared porous graphite as anode could be fully charged within 12 min (corresponding to 5 C charging rate). If such batteries were used as power sources of electric vehicles, they would become more acceptable by people.

Acknowledgments This investigation was supported by Microvast Inc. and was approved for publication.

References

1. Tarascon JM, Armand M (2001) *Nature* 414:359–367
2. Goodenough JB, Kim Y (2010) *Chem Mater* 22:587–603
3. Wu YP, Rahm E, Holze R (2003) *J Power Sources* 114:228–236
4. Marom R, Amalraj SF, Leifer N, Jacob D, Aurbach D (2011) *J Mater Chem* 21:9938–9954
5. Striebel KA, Shim J, Cairns EJ, Kostecki R, Lee YJ, Reimer J, Richardson TJ, Ross PN, Song X, Zhuang GV (2004) *J Electrochem Soc* 151:A857–A866
6. Zhang SS (2006) *J Power Sources* 161:1385–1391
7. Peled E, Menachem C, Bar-Tow D, Melman A (1996) *J Electrochem Soc* 143:L4–L7
8. Wu YP, Holze R (2003) *J Solid State Electrochem* 8:73–78
9. Nakajima T, Koh M, Singh RN, Shimada M (1999) *Electrochim Acta* 44:2879–2888
10. Yu P, Ritter JA, White RE, Popov BN (2000) *J Electrochem Soc* 147:1280–1285
11. Veeraraghavan B, Durairajan A, Haran B, Popov B, Guidotti R (2002) *J Electrochem Soc* 149:A675–A681
12. Yoshio M, Wang H, Fukuda K, Hara Y, Adachi Y (2000) *J Electrochem Soc* 147:1245–1250
13. Chang H, Bard AJ (1991) *J Am Chem Soc* 113:5588–5596
14. Lukas M, Meded V, Vijayaraghavan A, Song L, Ajayan PM, Fink K, Wenzel W, Krupke R (2013) *Nat Commun* 4:1379
15. Pan ZJ, Yang RT (1991) *J Catal* 130:161–172
16. Holstein WL, Boudart M (1982) *J Catal* 75:337–353
17. Deng TS, Zhou XP (2016) *Mater Lett* 176:151–154
18. Ferrari AC, Robertson J (2000) *Phys Rev B Condens Matter* 61:14095–14107
19. Menachem C, Peled E, Burstein L, Rosenberg Y (1997) *J Power Sources* 68:277–282
20. Kamisah MM, Munirah HS, Mansor MS (2007) *Ionics* 13:223–225
21. Zhang S, Shi PF (2004) *Electrochim Acta* 49:1475–1482
22. Bruce PG, Scrosati B, Tarascon JM (2008) *Angew Chem Int Ed* 47:2930–2946
23. Arico AS, Bruce P, Scrosati B, Tarasconand JM, VanSchalkwijk W (2005) *Nat Mater* 4:366–377
24. Zhang NX, Tang HQ (2012) *J Power Sources* 218:52–55